

Benchmarking Universal Machine Learning Interatomic Potentials for Supported Nanoparticles: Decoupling Energy Accuracy from Structural Exploration

Jiayan Xu,[†] Abhirup Patra,[‡] Amar Deep Pathak,[¶] Sharan Shetty,[¶] Detlef Hohl,[§]
and Roberto Car*,[†]

[†]*Department of Chemistry, Princeton University, Princeton, New Jersey 08544, United States*

[‡]*Shell International Exploration & Production Inc., 200 N Dairy Ashford Rd, Houston, Texas 77079, United States*

[¶]*Shell India Markets Pvt. Ltd. (Shell Projects & Technology), Mahadeva Kodigehalli, Bengaluru, 562149, Karnataka, India*

[§]*Shell Information Technology International Inc., 3333 Highway 6 South, Houston, Texas 77082, United States*

E-mail: rcar@princeton.edu

Abstract

Supported nanoparticle catalysts are widely used in the chemical industry. Computational modeling of supported nanoparticles based on density functional theory (DFT) often involves structural searches of stable local minimum energy configurations and molecular dynamics simulations at finite temperature. These are computationally demanding tasks that are intractable within DFT for large systems. In the last two decades, machine learning interatomic potentials (MLIPs) have been successfully used to substantially increase the size and time scales accessible to simulations that retain DFT accuracy. However, training reliable MLIPs is non-trivial as it requires many costly DFT calculations. Recently, several universal MLIPs (uMLIPs) have been developed, which are trained on large datasets that cover a wide range of molecules and materials. Here, we benchmark the accuracy and the efficiency of these uMLIPs in describing Cu nanoparticles supported on Al_2O_3 surfaces against our domain-specific DP-UniAlCu model. We find that the MACE-OMAT can reproduce reasonably well the low-energy configurations found in global optimization at an energy accuracy comparable to DP-UniAlCu. Interestingly, the MatterSim-v1.0.0-1M model, which exhibits larger deviations in the binding energies, can find even more stable configurations than the other two models in some supported nanoparticle sizes, showing its capability in structure exploration. For MD simulations, MACE-OMAT and MatterSim-v1.0.0-1M can qualitatively reproduce the mean-squared displacements of Cu atoms (MSD_{Cu}) predicted by DP-UniAlCu, albeit at roughly two orders of magnitude higher cost. We demonstrate that the uMLIPs can be very useful in simulating supported nanoparticles even without any fine-tuning, though their reduced efficiency remains a limiting factor for large-scale simulations.

Introduction

Atomic simulation is an indispensable tool in understanding various physical phenomena from an atomic perspective. Heterogeneous catalysis, a complex process that usually involves small molecules and solid surfaces, has benefited from valuable insights obtained from atomic simulation.¹ The proper description of catalytic reactions and catalyst structures requires a reliable method at the quantum mechanical level. Density functional theory (DFT) has been the workhorse for atomic simulation over the years. However, due to its intensive computational cost, DFT-based simulations cannot satisfy the growing interest in the realistic modeling of catalytic systems that require both extended spatial and time scales.²

Supported nanoparticle catalyst is one of the most widely used catalysts in the chemical industry.³ The computational modeling of supported nanoparticles often involves the structure search of stable configurations at 0 K and the molecular dynamics (MD) simulation at finite temperature. Both the structure search and the MD are computationally demanding and become intractable to DFT when the system size increases. The typical size of a supported nanoparticle synthesized in experiments is in the range of 1-10 nm, where a reasonable structure model of a 2-nm-sized nanoparticle together with the substrate may contain thousands of atoms. The supported nanoparticle structure adopted in DFT-based studies is usually a simplified model that only contains a few dozen atoms. Thus, the computational results are difficult to directly compare with experiments. To understand and design better supported nanoparticle catalysts computationally, an accurate and efficient simulation method is highly desirable.

In the last two decades, machine learning interatomic potentials (MLIPs) have been developed to accelerate atomic simulations, which retain DFT accuracy at a force-field-like cost, and find extensive applications in heterogeneous catalysis.⁴⁻⁶ However, the development of an MLIP is a non-trivial task, which requires the user to collect a large amount of *ab initio* data through many training-validation-application cycles. Also, the MLIP is usually specific to one system, and its transferability is limited. For example, an MLIP trained

on one crystalline phase may be useful for exploring configurations of another phase, but the energy and the forces are normally less accurate. Recently, several universal MLIPs (uMLIPs) have emerged, namely, DPA2,⁷ DPA3,⁸ MACE-MP,⁹ and MatterSim.¹⁰ These uMLIPs are trained on large datasets that cover a wide range of molecules and materials, such as Materials Project (MP),¹¹ Open Catalyst Project (OC2M),¹² and Open Materials Dataset (OMAT),¹³ and are expected to apply to a wide range of systems. In general, uMLIPs provide a good foundation to develop an MLIP for a specific system since they can generate reasonable configurations without active learning and can be further fine-tuned to a target accuracy if necessary. MACE-MP⁹ has been tested on numerous systems from solid materials to heterogeneous interfaces, while other recent uMLIPs have been mainly tested with solid-state systems. Despite all the tests that have been done, the benchmark of the uMLIPs on supported nanoparticles is still lacking.

In this work, we examined several uMLIPs on simulating supported nanoparticles, where two main application scenarios are demonstrated: (1) global optimization that produces low-energy configurations of nanoparticles serving good initial structures for the further investigation of dynamics, and (2) MD that reveals the dynamics of supported nanoparticles at finite temperature. We choose Cu nanoparticles on Al_2O_3 surfaces as the benchmark system and set the domain-specific deep potential (DP) model developed in our previous work¹⁴ as the benchmark baseline, which is denoted as DP-UniAlCu in the following sections. The DP-UniAlCu model is trained on a dataset named UniAlCu, including various structures of supported Cu nanoparticles on Al_2O_3 surfaces. The uMLIPs examined by this work include DPA2 (mptrj and oc20),⁷ DPA3 (omat24),⁸ MACE-MP (medium),⁹ MACE-OMAT (medium),¹³ and MatterSim (v1.0.0-1M and v1.0.0-5M).¹⁰

Results

Minimum Energy Configurations from Cu₁ to Cu₂₁. We commence our examination with geometric optimization-based tasks. **Figure 1** shows the binding energy (defined in **Equation 1**) of Cu_{1–21} on three Al₂O₃ surfaces by various MLIPs, which are obtained from global optimization in our previous work.¹⁴ The three Al₂O₃ surfaces are modeled by $p(3 \times 2)$ γ -Al₂O₃(100), $p(2 \times 2)$ γ -Al₂O₃(110), $p(3 \times 2\sqrt{3})$ α -Al₂O₃(0001) periodic slabs (**Figure S1**). The comparison of the absolute total energy is not accessible as these MLIPs are trained on datasets labelled by different DFT calculation settings. The Perdew-Burke-Ernzerhof (PBE) exchange-correlation functional is used for the reported DFT binding energy results and also the dataset to train our DP-UniAlCu model. MACE and MatterSim-branched uMLIPs are trained on datasets labelled by DFT-PBE using a similar setting as ours (**Table S1 and S2**), which is the default one named as “MPRelaxSet” used in Materials Project.^{11,15} The binding energy results from our DFT setting and “MPRelaxSet” is almost identical with a maximum absolute error of 0.10 eV (**Figure S2**). Since all MLIPs tested here are trained on DFT-PBE, we are able to examine the accuracy of these MLIPs on the binding energy, where a reliable MLIP should be able to reproduce the binding energy trend across different nanoparticle sizes and surfaces. We noticed the dispersion interaction may affect the absolute values of binding energies of supported nanoparticles when compared to experiments,^{16,17} however, the DFT-PBE results presented here only served as a reference for the comparison of different MLIPs and the relative binding strength across different nanoparticle sizes and supporting surfaces is preserved.¹⁴ **Figure 1a-c** show the binding energy results of Cu_{1–21} on γ -Al₂O₃(100), γ -Al₂O₃(110), and α -Al₂O₃(0001), respectively. The MLIP binding energy results are calculated based on the MLIP total energies of the configurations minimized by the corresponding MLIP model starting from the DFT-minimized configurations. No significant structural difference between DFT and MLIP-minimized configurations is observed. Most models give minimized structures with an averaged atomic displacement smaller than ~ 0.05 Å compared to the DFT-minimized structures except for DPA2-MPTrj and DPA2-OC2M

that give displacements larger than $\sim 0.1 \text{ \AA}$ (**Figure S3**). All examined uMLIPs can reproduce the binding energy trend as a function of the nanoparticle size on a single Al_2O_3 surface, namely, the binding energy on $\gamma\text{-Al}_2\text{O}_3(100)$ is almost independent of the nanoparticle size while the binding energies on $\gamma\text{-Al}_2\text{O}_3(110)$ and $\alpha\text{-Al}_2\text{O}_3(0001)$ decrease significantly with the nanoparticle size. When comparing the binding energies of the same nanoparticle size across different Al_2O_3 surfaces, some uMLIPs cannot capture the relative binding strength to the supporting surface, where the trend by DFT-PBE from the strongest to the weakest should be $\gamma\text{-Al}_2\text{O}_3(110)$, $\gamma\text{-Al}_2\text{O}_3(100)$, and $\alpha\text{-Al}_2\text{O}_3(0001)$. For example, DPA2-MPTrj predicts a stronger binding on $\alpha\text{-Al}_2\text{O}_3(0001)$ than on $\gamma\text{-Al}_2\text{O}_3(110)$, which is inconsistent with DFT-PBE. **Figure 1d** shows the distribution of binding energy errors through the violin plots, where a good model should have an error distribution centered at zero with a small spread. The binding energy error is defined as the difference between the binding energy predicted by an MLIP and the binding energy by DFT-PBE. MACE-OMAT and MatterSim-v1.0.0-5M exhibit small errors with narrow spreads centered near zero, which reproduce both the relationship between the binding energy and the nanoparticle size and the relative binding strength across three Al_2O_3 surfaces. It is surprising that MACE-OMAT and MatterSim-v1.0.0-5M are not trained explicitly on any structures of supported nanoparticles but have an accuracy comparable to our DP-UniAlCu model. MACE-MP, which has the same architecture as MACE-OMAT but is trained on a smaller dataset, is less accurate than MACE-OMAT and predicts more negative binding energies on all three Al_2O_3 surfaces, which can be seen from the average binding energy errors. MatterSim-v1.0.0-1M, which is trained on the same dataset as MatterSim-v1.0.0-5M but has a smaller number of model parameters, leads to a degraded accuracy on binding energy, particularly for $\gamma\text{-Al}_2\text{O}_3(110)$ with the averaged binding energy error of $\sim 2 \text{ eV}$. The above results indicate that the model performance can be improved either by increasing the dataset size (MACE-MP vs. MACE-OMAT) or by increasing the model size (MatterSim-v1.0.0-1M vs. MatterSim-v1.0.0-5M). To examine this model improvement strategy, we trained a MACE model based on our

UniAlCu dataset using the same architecture as MACE-OMAT, which is denoted as the MACE-UniAlCu. The details of the training settings and the model errors on the entire UniAlCu dataset are given in **Section S3**. MACE-UniAlCu exhibits smaller error spreads for all three Al_2O_3 surfaces compared to both DP-UniAlCu and MACE-OMAT. The DPA2-MPTrj shows much larger errors compared to other MLIP models. The large errors are also observed for the DPA2-OC2M (**Figure S5**), which is trained on the OC2M dataset.¹⁸ The DPA3-OMAT exhibits smaller errors than DPA2-MPTrj and DPA2-OC2M due to its improved architecture. The model architecture can affect the accuracy, as seen from that DPA2-MPTrj is the head trained on the same dataset as MACE-MP, but has larger errors, which is similar in the case of DPA3-OMAT and MACE-OMAT. In addition, the multi-head training strategy used in DPA2 and DPA3, despite utilizing available datasets to the maximum extent, compromises the accuracy of a specific head due to inconsistent DFT settings in the datasets.

Global Optimization of Larger Nanoparticles. In practice, the global minimum configurations of supported nanoparticles are not available and are usually difficult to construct manually. Global optimization can explore low-energy configurations and possibly find the global minimum configurations of supported nanoparticles, where the initial structures are randomly generated, and the final structures can have different geometries but similar energies. A good MLIP should be able to minimize the initial random structures that may have unphysically short interatomic distances and distinguish the low-energy configurations from the high-energy ones. Therefore, global optimization is a good test for the uMLIPs to examine their stability in minimization and their performance in finding low-energy configurations. Based on the performance of uMLIPs on the binding energies of Cu_{1-21} , we examined MACE-OMAT and MatterSim-V1.0.0-1M due to their balance in accuracy and efficiency. At the same time, we tested DP-UniAlCu as a baseline. The global optimization based on the genetic algorithm was performed for several larger nanoparticles, including Cu_{27} , Cu_{38} , Cu_{47} and Cu_{55} . All the combinations of nanoparticle sizes and Al_2O_3

surfaces are not included in our UniAlCu dataset, making these global optimization tasks good examinations for the model’s extrapolation ability. The periodic slabs of $p(5 \times 3)$ γ - $\text{Al}_2\text{O}_3(100)$, $p(3 \times 3)$ γ - $\text{Al}_2\text{O}_3(110)$, $p(5 \times 3\sqrt{3})$ α - $\text{Al}_2\text{O}_3(0001)$ shown in **Figure S6** are used to accommodate the nanoparticles. In the global optimization task, the initial structures are randomly generated, and the structures in the following 20 generations are generated based on cut-and-splice and mutation algorithms, where the population size is set to 50. The details of the genetic algorithm are given in **Section Methods**. Among all obtained MLIP-minimized configurations, 50 structures with the lowest energies are further optimized by DFT. For the three MLIPs examined on one nanoparticle-surface combination, there will be 150 DFT-minimized configurations in total, forming the low-energy ensemble.

Table 1 gives the error distributions on the low-energy ensembles. For nanoparticles on the two γ - Al_2O_3 surfaces, our DP-UniAlCu model and the MACE-OMAT model have smaller error spreads compared to MatterSim-v1.0.0-1M. Our DP-UniAlCu is slightly better as the MACE-OMAT model gives more negative binding energies and exhibits larger error spreads, for example, Cu_{38} on γ - $\text{Al}_2\text{O}_3(100)$. The Mattersim-v1.0.0-1M model gives significantly large errors for Cu_{27} , Cu_{38} , and Cu_{47} on two γ - Al_2O_3 surfaces and predicts decreasing trends in the binding energy, while it gives results of Cu_{55} closer to DFT. This non-uniform accuracy indicates that the extrapolation ability of a uMLIP can be strongly system-dependent and cannot be guaranteed for consistency across systems, which may be rooted deeply in their training datasets. The DP-UniAlCu and MACE-OMAT models exhibit similar non-uniform accuracies but less severe, for example, they are slightly less accurate for two γ - Al_2O_3 surfaces than α - $\text{Al}_2\text{O}_3(0001)$. Though large offsets are observed, the error spreads by MatterSim-v1.0.0-1M are generally small, indicating the relative stability of the low-energy configurations may pertain. For α - $\text{Al}_2\text{O}_3(0001)$, all three models exhibit larger error spreads. The error averages by DP-UniAlCu and MACE-OMAT are close to zero, while the error average by MatterSim-v1.0.0-1M is around +2 eV. For Cu_{47} and Cu_{55} , MACE-OMAT performs better than DP-UniAlCu, showing smaller error spreads.

In practice, the low-energy candidates generated by MLIP can be further verified by DFT to find the global minimum configuration, thus, whether the DFT-minimized global minimum configuration is included in the low-energy ensemble is a good indicator of the MLIP performance. Two metrics (**Table 2**) are used to quantify the quality of an MLIP-generated low-energy ensemble, namely, rank biased overlap¹⁹ (RBO, defined in **Equation 2**) and Kendall’s τ ²⁰ (defined in **Equation 3**). The RBO measures the similarity between two lists of binding energies, the DFT ones and the MLIP ones, and focuses more on the top of the lists, where a larger RBO value indicates a better MLIP performance. However, it is less sensitive to the order of the binding energies in the lists. In addition, Kendall’s τ measures the ordinal association between two lists of binding energies, where a larger value indicates a better MLIP performance. In seven out of twelve systems, our DP-UniAlCu model shows the best performance in both RBO and Kendall’s τ , indicating its excellent ability to generate low-energy ensembles consistent with DFT. For the rest of the systems, MACE-OMAT performs better than DP-UniAlCu. MatterSim-v1.0.0-1M gives less satisfactory results and only exhibits comparable performance on a few systems, such as Cu₄₇ on γ -Al₂O₃(100) and Cu₅₅ on γ -Al₂O₃(110). Combining the energetic and ranking metrics, DP-UniAlCu is the most reliable one in the global optimization task, and MACE-OMAT can be a good alternative.

For better visualization of the low-energy ensembles by different MLIPs, the energy spectra of the low-energy ensembles for nanoparticles on three Al₂O₃ surfaces are shown in **Figure 2a-c** for Cu₂₇ and Cu₃₈ and in **Figure 3a-c** for Cu₄₇ and Cu₅₅. All binding energies are referenced to the binding energy of the corresponding DFT-minimized global minimum configuration as $E_b - \min(E_b^{\text{DFT}})$. The configurations from different MLIP-based global optimization are marked by different colors, namely, blue for DP-UniAlCu, green for MACE-OMAT, and orange for MatterSim-v1.0.0-1M. The arrows indicate the positions of the DFT-minimized global minimum configurations in spectra, which have the color of the MLIP generating the corresponding configuration. The DFT-minimized global minimum configuration tasks are mainly from global optimizations by our DP-UniAlCu model except

for $\text{Cu}_{47}/\gamma\text{-Al}_2\text{O}_3(100)$, $\text{Cu}_{38}/\gamma\text{-Al}_2\text{O}_3(110)$, $\text{Cu}_{47}/\alpha\text{-Al}_2\text{O}_3(0001)$ by Mattersim-v1.0.0-1M, and $\text{Cu}_{27}/\alpha\text{-Al}_2\text{O}_3(0001)$ by MACE-OMAT. Though the DFT-minimized global minimum configurations originated from other MLIPs are not directly found by DP-UniAlCu, they are always among the fifty lowest energy configurations in the spectra by DP-UniAlCu and are very likely to be found if more structures are explored. For MACE-OMAT, it predicts the DFT-minimized global minimum configurations in the lower energy parts of its energy spectra for the most systems while in the higher energy parts for some systems such as $\text{Cu}_{38}/\gamma\text{-Al}_2\text{O}_3(100)$ and $\text{Cu}_{27}/\gamma\text{-Al}_2\text{O}_3(110)$, indicating it may require more MACE-OMAT-generated configurations to be verified by DFT to find the DFT-minimized global minimum configuration. Interestingly, MatterSim-v1.0.0-1M exhibits larger deviations in binding energies than both DP-UniAlCu and MACE-OMAT as shown in **Figure 1**, but it may still find the DFT-minimized global minimum configuration in its low-energy ensemble and even discover more stable configurations than the other two models. This indicates that the MLIP’s exploration ability in the configuration space may not solely be characterized by the error metrics on a preset dataset, and a model with less satisfying metrics can be useful in structure search, such as global optimization.

Finite-Temperature Dynamics. The dynamic behavior of supported nanoparticles is important for understanding the catalytic activity and stability. Several MD-based tasks are designed to examine uMLIPs. We first tested the mean-squared displacements of Cu atoms (MSD_{Cu} , defined in **Equation 4**) of Cu_{13} on three Al_2O_3 surfaces with short-time MD simulations, where *ab initio* MD (AIMD) trajectories are available for reference. The DP-UniAlCu, MACE-UniAlCu, MACE-OMAT, MatterSim-v1.0.0-1M, MatterSim-v1.0.0-5M, and DPA3-OMAT are tested. For each MLIP, 20 MD simulations starting from the same global minimum configuration but initialized from different velocities by Maxwell-Boltzmann distribution at 800 K are performed for 20 ps with a timestep of 2 fs. For AIMD, only one trajectory is performed with the same settings. The window-averaged MSD_{Cu} up to 5 ps are shown in **Figure 4a-c**. The vertical bars are the standard deviations of 20 MD simulations by

MLIPs. The model accuracy can be examined by checking whether the AIMD results fall within the standard deviations of MLIPs. For $\gamma\text{-Al}_2\text{O}_3(100)$, all models except for MACE-OMAT and DPA3-OMAT give MSD_{Cu} results that are close to the AIMD results, which exhibit smaller MSD_{Cu} values. For $\gamma\text{-Al}_2\text{O}_3(110)$, all models give consistent results with AIMD. For $\alpha\text{-Al}_2\text{O}_3(0001)$, all models except for two MatterSim models produce MSD_{Cu} results closer to AIMD, which show larger MSD_{Cu} values. The radial distribution functions (RDFs) of Cu-Al and Cu-O pairs are shown in **Figure 4d-f** and **Figure 4g-i**, respectively, which are averaged over snapshots every 0.1 ps from 0.2 ps to 20 ps. The RDFs of Cu-Al and Cu-O by DP-UniAlCu, MACE-UniAlCu and MACE-OMAT are in good agreement with the AIMD results, while other models give larger deviations. The RDF of Cu-Cu can be well reproduced by all models (**Figure S7**). Since the 20-ps-long MD simulations are too short to observe any diffusion of the entire nanoparticle, we performed 1-ns-long MD simulations for Cu_{13} on three $\alpha\text{-Al}_2\text{O}_3(0001)$ surfaces with DP-UniAlCu, MACE-UniAlCu, MACE-OMAT, MatterSim-v1.0.0-1M, and DPA3-OMAT to investigate the long-time dynamic behavior. Five independent MD simulations are performed for each MLIP starting from the same global minimum configuration but initialized from different velocities by Maxwell-Boltzmann distribution at 800 K. The results of MSD_{Cu} up to 100 ps for Cu_{13} on three Al_2O_3 surfaces are shown in **Figure 5a-c**. The vertical bars are the standard deviations of five MD simulations by MLIPs. Since ns-long MD simulations are not readily accessible to AIMD, the benchmark here only served as a cross-validation across different MLIPs by comparing results against our DP-UniAlCu model. Overall, all MLIPs predict qualitatively consistent mobility trend of Cu atoms on three Al_2O_3 surfaces, where the MSD_{Cu} on $\gamma\text{-Al}_2\text{O}_3(100)$ and $\alpha\text{-Al}_2\text{O}_3(0001)$ are comparable and larger than $\gamma\text{-Al}_2\text{O}_3(110)$. MatterSim-v1.0.0-1M gives slightly larger MSD_{Cu} for Cu_{13} on $\gamma\text{-Al}_2\text{O}_3(100)$ and $\gamma\text{-Al}_2\text{O}_3(110)$, and much larger MSD_{Cu} for $\alpha\text{-Al}_2\text{O}_3(0001)$ compared to DP-UniAlCu. MACE-OMAT gives almost identical MSD_{Cu} for Cu_{13} on $\gamma\text{-Al}_2\text{O}_3(110)$ as DP-UniAlCu while more deviations between them are observed for Cu_{13} on $\gamma\text{-Al}_2\text{O}_3(100)$ and $\alpha\text{-Al}_2\text{O}_3(0001)$, where MACE-OMAT gives smaller MSD_{Cu}

values. By using the MACE-UniAlCu model, which is trained on the same dataset as DP-UniAlCu, the MSD_{Cu} results for $\gamma\text{-Al}_2\text{O}_3(100)$ and $\alpha\text{-Al}_2\text{O}_3(0001)$ become closer to those by DP-UniAlCu, however, a smaller MSD_{Cu} is observed for $\gamma\text{-Al}_2\text{O}_3(110)$. DPA3-OMAT exhibits a consistent mobility trend as DP-UniAlCu but gives smaller MSD_{Cu} values for all three Al_2O_3 surfaces. To perform a more quantitative comparison, more simulations with a longer time are necessary, which can be challenging for uMLIPs. The computation performance is shown in **Figure 5d**, which is taken from the 100-ps simulation of an FCC Cu bulk with 2048 atoms. All models are performed on a single NVIDIA 80G A100 GPU with LAMMPS²¹ except for MatterSim-v1.0.0-1M with ASE.²² Our DP-UniAlCu model is about two orders faster than other models, achieving the best balance between accuracy and efficiency here. The reduced efficiency of the uMLIPs arises from their large parameter counts, the overhead associated with message passing, and the substantial cost of tensor products when equivariant features are employed.²³ Though quantitative results for large size and time scales may not be obtained directly by uMLIPs, they are useful models to sample configuration spaces of interest, which can be distilled by cheaper models realizing long-time simulations.

Discussion and Conclusion

In this work, we tested several uMLIPs on supported Cu nanoparticles on Al_2O_3 surfaces and found that they can be very useful in simulating supported nanoparticles even without any fine-tuning, including the global optimization of low-energy configurations and the MD at finite temperature.

The uMLIPs examined in this work can produce reasonable results on the binding energies of small supported nanoparticles (Cu_{1-21}) reported in our previous study,¹⁴ where MACE-OMAT shows an accuracy comparable to our domain-specific DP-UniAlCu model. In the global optimization of larger supported nanoparticles (Cu_{27} , Cu_{38} , Cu_{47} , and Cu_{55}), our DP-UniAlCu model behaves better than MACE-OMAT and Mattersim-v1.0.0-1M in finding low-energy minimum configurations. Interestingly, Mattersim-v1.0.0-1M, which shows larger deviations in binding energies, can find even more stable configurations than the other two models in some systems, indicating its exploration ability in the configuration space is not solely characterized by the error metrics on a preset dataset. Alongside the exploration ability of MatterSim-v1.0.0-1M, the non-uniform accuracy across different systems is observed, for instance, the binding energy accuracy in one nanoparticle size is better than another size on the same Al_2O_3 surface. This non-uniform accuracy may be due to the imbalance in the number of configurations from different systems, where the initial dataset is made up of configurations from one specific system and the configurations of other systems are accumulated in active learning. In terms of global optimization, since the system size of interest is usually accessible to DFT, the MLIP-generated configurations can still be verified by DFT to find the global minimum configurations. The model’s stability in generating diverse configurations in a large region of the configuration space is more important than the accuracy of the energy, as it provides more candidates for DFT verification. A model with better accuracy can improve the performance in the workflow of global optimization since it can produce more low-energy configurations close to the DFT global minimum and reduce the number of DFT calculations, however, the improved accuracy generally comes with an

increased computational cost. Though minimization is fast for a single structure and can be made parallel, the computational cost can become intensive for complex systems even by MLIPs, where numerous structures are calculated.

The benchmark on the MD of supported nanoparticles shows that the uMLIPs can produce consistent results of MSD_{Cu} and RDF in 20-ps-long simulations compared to AIMD. When it comes to long-time MD simulations, it becomes challenging in two aspects: the lack of DFT reference and the computational cost. The property predicted by MLIPs in the long-time limit can only be cross-validated by different models in the absence of AIMD. MACE-OMAT and MatterSim-v1.0.0-1M exhibit qualitative trends in MSD_{Cu} up to 100 ps, which are similar to our DP-UniAlCu model and the MACE-UniAlCu trained on our dataset. To obtain more quantitative results, longer MD simulations are required but not feasible for uMLIPs. Our DP-UniAlCu model is about two orders of magnitude faster than MACE-OMAT and Mattersim-v1.0.0-1M, which makes it a good candidate for long-time MD simulations. Currently, the best tradeoff in accuracy and efficiency is still obtained within the DP architecture. The accuracy of DP can be improved by message passing as demonstrated with DP-MP²⁴ and the efficiency is not degraded as much as switching to uMLIPs. Nevertheless, the uMLIPs can be an alternative method to generate configurations through MD simulations for the initial dataset in the MLIP development instead of the perturbation of a few given structures.²⁵ For example, distillation is a promising strategy to alleviate the computational performance issue of uMLIPs by training a cheaper model on the configurations sampled and labelled by a uMLIP.

The emergence of uMLIPs provides a good foundation to develop domain-specific MLIPs for complex systems, however, the challenges still exist in reducing the computational cost and integrating fine-tuning and distillation in the current framework of active learning. We expect the benchmarks in this work can provide valuable insights into the applications of uMLIPs for a better understanding of supported nanoparticle catalysts.

Methods

The DFT calculations used in binding energy computation and ab initio molecular dynamics are performed with the Vienna Ab initio Simulation Package (VASP).^{26,27} The Perdew-Burke-Ernzerhof (PBE) approximation for the exchange-correlation functional²⁸ is used in our UniAlCu dataset and in calculating the binding energies of supported nanoparticles. The MACE-MP, MACE-OMAT, MatterSim-v1.0.0-1M, and MatterSim-v1.0.0-5M are trained on the PBE-based datasets with slightly different parameters. The detailed comparison of input settings can be found in **Section S2**. The MACE-UniAlCu model is trained on our UniAlCu dataset using the same setting as MACE-OMAT, which is discussed in **Section S3**.

The simulations by uMLIPs are performed with either LAMMPS²¹ or ASE²² through interfaces implemented in the GDPy package.²⁹ The global optimization is based on the genetic algorithm implemented in the GDPy package,^{29,30} where the crossover used a cut-and-splice algorithm^{31,32} and the mutations include the rattle and mirror operations with equal probabilities. The population size is set to 50 and the number of generations is set to 20. The configurations in the first generation are randomly generated, and those in the following generations are produced by the crossover and mutation methods.

The binding energy E_b of a supported nanoparticle is defined as

$$E_b = E_{\text{Cu}_N/\text{surf}} - E_{\text{surf}} - E_{\text{Cu}_N} \quad (1)$$

where $E_{\text{Cu}_N/\text{surf}}$ is the potential energy of a Cu nanoparticle on an Al_2O_3 surface, E_{surf} is the potential energy of a pristine Al_2O_3 surface, and E_{Cu_N} is the potential energy of the global minimum configuration of Cu_N in the gas phase.

Two ranking metrics are used to quantify the quality of an MLIP-generated low-energy ensemble. The rank based overlap (RBO)¹⁹ is defined as

$$q(S, T, p) = (1 - p) \sum_{d=1}^{\infty} p^{d-1} \frac{|S_{1:d} \cap T_{1:d}|}{d}, \quad (2)$$

where S and T are two lists of binding energies ranked from low to high, d is the length of a sub-list, and p is a parameter controlling the top-weightness and chosen to be 0.94 when 95% of the weight is contributed by the top fifty energies. The Kendall's τ ²⁰ is defined as

$$\tau = \frac{P - Q}{\sqrt{(P + Q + T)(P + Q + U)}} \quad (3)$$

where P is the number of concordant pairs, Q is the number of discordant pairs, T is the number of ties only in the first list, and U is the number of ties only in the second list.

The mean-squared displacements of Cu atoms (MSD_{Cu}) is given by

$$\text{MSD}(t; r) = \langle \frac{1}{N} \sum_{i=1}^N \|r(t + \tau) - r(\tau)\|^2 \rangle_{\tau} , \quad (4)$$

where N is the number of Cu atoms, $r(t)$ is the coordinate at timestep t , τ is the time origin, and $\langle \dots \rangle_{\tau}$ denotes the average over all time origins with a lagtime in one trajectory.

Acknowledgement

The funding for this project was provided by Shell International Exploration and Production Inc., USA. The calculations were performed largely using the Princeton Research Computing resources at Princeton University. The authors also acknowledge the computing resources from the National Energy Research Scientific Computing Center (NERSC) operated under Contract No. DE-AC0205CH11231 using NERSC award ERCAP0021510. The software used in the present work has been developed in the Computational Chemical Science Center “Chemistry in Solution and at Interfaces (CSI)” funded by the USA Department of Energy under award DE-SC0019394. RC was partially supported by this grant, and JX benefited of scientific discussions with the members of CSI.

Supporting Information Available

7 figures, 2 tables, notes and references

References

- (1) Chen, B. W.; Xu, L.; Mavrikakis, M. Computational methods in heterogeneous catalysis. *Chem. Rev.* **2020**, *121*, 1007–1048.
- (2) Grajciar, L.; Heard, C. J.; Bondarenko, A. A.; Polynski, M. V.; Meeprasert, J.; Pidko, E. A.; Nachtigall, P. Towards operando computational modeling in heterogeneous catalysis. *Chem. Soc. Rev.* **2018**, *47*, 8307–8348.
- (3) Liu, L.; Corma, A. Metal catalysts for heterogeneous catalysis: from single atoms to nanoclusters and nanoparticles. *Chem. Rev.* **2018**, *118*, 4981–5079.
- (4) Cheng, X.; Wu, C.; Xu, J.; Han, Y.; Xie, W.; Hu, P. Leveraging machine learning potentials for in-situ searching of active sites in heterogeneous catalysis. *Precis. Chem.* **2024**, *2*, 570–586.
- (5) Omranpour, A.; Elsner, J.; Lausch, K. N.; Behler, J. Machine learning potentials for heterogeneous catalysis. *ACS Catal.* **2025**, *15*, 1616–1634.
- (6) Xia, J.; Zhang, Y.; Jiang, B. The evolution of machine learning potentials for molecules, reactions and materials. *Chem. Soc. Rev.* **2025**,
- (7) Zhang, D.; Liu, X.; Zhang, X.; Zhang, C.; Cai, C.; Bi, H.; Du, Y.; Qin, X.; Peng, A.; Huang, J.; others DPA-2: a large atomic model as a multi-task learner. *npj Comput. Mater.* **2024**, *10*, 293.
- (8) Zhang, D.; Peng, A.; Cai, C.; Li, W.; Zhou, Y.; Zeng, J.; Guo, M.; Zhang, C.; Li, B.; Jiang, H.; others Graph neural network model for the era of large atomistic models. *arXiv preprint arXiv:2506.01686* **2025**,
- (9) Batatia, I.; Benner, P.; Chiang, Y.; Elena, A. M.; Kovács, D. P.; Riebesell, J.; Advincula, X. R.; Asta, M.; Avaylon, M.; Baldwin, W. J.; others A foundation model for atomistic materials chemistry. *J. Chem. Phys.* **2025**, *163*.

- (10) Yang, H.; Hu, C.; Zhou, Y.; Liu, X.; Shi, Y.; Li, J.; Li, G.; Chen, Z.; Chen, S.; Zeni, C.; others Mattersim: A deep learning atomistic model across elements, temperatures and pressures. *arXiv:2405.04967* **2024**,
- (11) Jain, A.; Ong, S. P.; Hautier, G.; Chen, W.; Richards, W. D.; Dacek, S.; Cholia, S.; Gunter, D.; Skinner, D.; Ceder, G.; others Commentary: The Materials Project: A materials genome approach to accelerating materials innovation. *APL Mater.* **2013**, *1*.
- (12) Tran, R.; Lan, J.; Shuaibi, M.; Wood, B. M.; Goyal, S.; Das, A.; Heras-Domingo, J.; Kolluru, A.; Rizvi, A.; Shoghi, N.; others The Open Catalyst 2022 (OC22) dataset and challenges for oxide electrocatalysts. *ACS Catal.* **2023**, *13*, 3066–3084.
- (13) Barroso-Luque, L.; Shuaibi, M.; Fu, X.; Wood, B. M.; Dzamba, M.; Gao, M.; Rizvi, A.; Zitnick, C. L.; Ulissi, Z. W. Open Materials 2024 (OMat24) Inorganic Materials Dataset and Models. 2024.
- (14) Xu, J.; Das, S.; Pathak, A. D.; Patra, A.; Shetty, S.; Hohl, D.; Car, R. Dynamic metal-support interaction dictates Cu nanoparticle sintering on Al₂O₃ surfaces. *ACS Nano* **2025**, *19*, 29242–29254.
- (15) Python Materials Genomics (pymatgen): A robust, open-source python library for materials analysis. *Comput. Mater. Sci.* **2013**, *68*, 314–319.
- (16) Wellendorff, J.; Silbaugh, T. L.; Garcia-Pintos, D.; Nørskov, J. K.; Bligaard, T.; Studt, F.; Campbell, C. T. A benchmark database for adsorption bond energies to transition metal surfaces and comparison to selected DFT functionals. *Surf. Sci.* **2015**, *640*, 36–44.
- (17) Zhao, K.; Auerbach, D. J.; Campbell, C. T. Predicting adhesion energies of metal nanoparticles to support surfaces, which determines metal chemical potential versus particle size and thus catalyst performance. *ACS Catal.* **2024**, *14*, 12857–12864.

- (18) Chanussot, L. et al. Open Catalyst 2020 (OC20) Dataset and Community Challenges. *ACS Catal.* **2021**, *11*, 6059–6072.
- (19) Webber, W.; Moffat, A.; Zobel, J. A similarity measure for indefinite rankings. *ACM Transactions on Information Systems (TOIS)* **2010**, *28*, 1–38.
- (20) Kendall, M. G. The treatment of ties in ranking problems. *Biometrika* **1945**, *33*, 239–251.
- (21) Thompson, A. P.; Aktulga, H. M.; Berger, R.; Bolintineanu, D. S.; Brown, W. M.; Crozier, P. S.; In’t Veld, P. J.; Kohlmeyer, A.; Moore, S. G.; Nguyen, T. D.; others LAMMPS-a flexible simulation tool for particle-based materials modeling at the atomic, meso, and continuum scales. *Comput. Phys. Commun.* **2022**, *271*, 108171.
- (22) Larsen, A. H.; Mortensen, J. J.; Blomqvist, J.; Castelli, I. E.; Christensen, R.; Dułak, M.; Friis, J.; Groves, M. N.; Hammer, B.; Hargus, C.; others The atomic simulation environment-a Python library for working with atoms. *J. Phys.: Condens. Matter* **2017**, *29*, 273002.
- (23) Batatia, I.; Batzner, S.; Kovács, D. P.; Musaelian, A.; Simm, G. N.; Drautz, R.; Ortner, C.; Kozinsky, B.; Csányi, G. The design space of E (3)-equivariant atom-centred interatomic potentials. *Nature Machine Intelligence* **2025**, *7*, 56–67.
- (24) Gao, R.; Li, Y.; Car, R. Enhanced deep potential model for fast and accurate molecular dynamics: application to the hydrated electron. *Phys. Chem. Chem. Phys.* **2024**, *26*, 23080–23088.
- (25) Zhang, L.; Lin, D.-Y.; Wang, H.; Car, R.; Weinan, E. Active learning of uniformly accurate interatomic potentials for materials simulation. *Phys. Rev. Mater.* **2019**, *3*, 023804.

- (26) Kresse, G.; Furthmüller, J. Efficiency of ab-initio total energy calculations for metals and semiconductors using a plane-wave basis set. *Comput. Mater. Sci.* **1996**, *6*, 15–50.
- (27) Kresse, G.; Furthmüller, J. Efficient iterative schemes for ab initio total-energy calculations using a plane-wave basis set. *Phys. Rev. B* **1996**, *54*, 11169.
- (28) Perdew, J. P.; Burke, K.; Ernzerhof, M. Generalized gradient approximation made simple. *Phys. Rev. Lett.* **1996**, *77*, 3865.
- (29) Xu, J. GDPy: Generating Deep Potential with Python. 2025; <https://github.com/hsulab/GDPy>.
- (30) Lee, M.-H.; Xu, J.; Xie, W. Exploring the Stability of Single-Atom Catalysts Using the Density Functional Theory-Based Global Optimization Method: H₂ Formation on VO_x/γ-Al₂O₃(100). *J. Phys. Chem. C* **2022**, *126*, 6973–6981.
- (31) Deaven, D. M.; Ho, K.-M. Molecular geometry optimization with a genetic algorithm. *Phys. Rev. Lett.* **1995**, *75*, 288.
- (32) Vilhelmsen, L. B.; Hammer, B. Systematic study of Au₆ to Au₁₂ gold clusters on MgO (100) F centers using density-functional theory. *Phys. Rev. Lett.* **2012**, *108*, 126101.

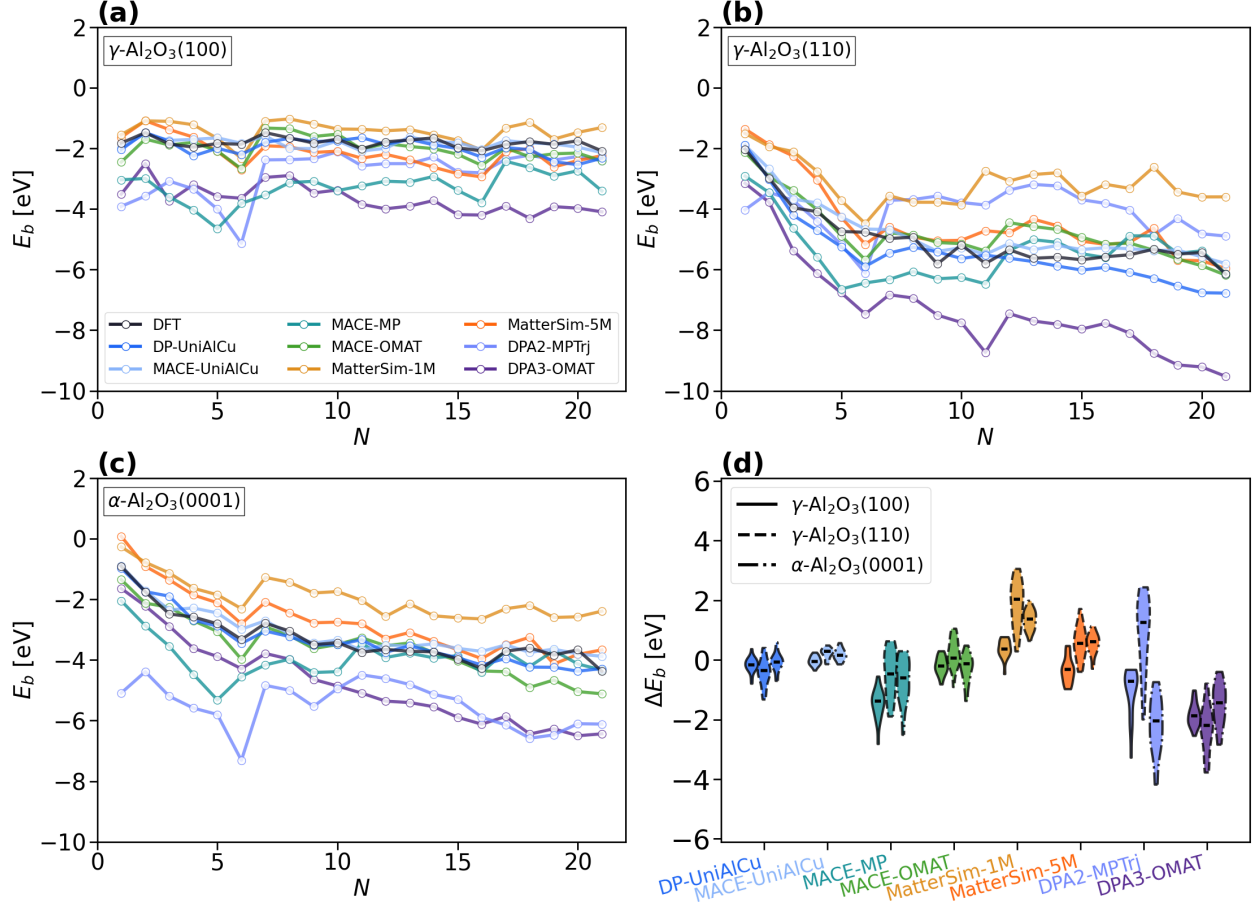


Figure 1: Several MLIPs are examined for the binding energies of Cu_{1-21} on three Al_2O_3 surfaces: (a) $\gamma\text{-Al}_2\text{O}_3(100)$ (b) $\gamma\text{-Al}_2\text{O}_3(110)$ (c) $\alpha\text{-Al}_2\text{O}_3(0001)$ (d) violin plots of errors in binding energy. DP-UniAlCu and MACE-UniAlCu have smaller spreads on the binding energy errors since they are specifically trained on these systems. Among uMLIPs, MACE-OMAT and MatterSim-v1.0.0-5M show similar accuracy as DP-UniAlCu, which reproduce the relative binding strength across three surfaces. Degraded performance is observed for MACE-MP and MatterSim-v1.0.0-1M as the former one is trained on a smaller dataset and the latter one is a model with smaller parameters. DPA2-MPTrj shows large energy differences compared to DFT and DPA3-OMAT has reduced errors due to its improved architecture.

Table 1: Energetics of Global Minimum Configurations (units in eV)

Model		DP-UniAlCu		MACE-OMAT		MatterSim-v1.0.0-1M	
Surface	Size	$avg(\Delta E_b) \downarrow$	$std(\Delta E_b) \downarrow$	$avg(\Delta E_b) \downarrow$	$std(\Delta E_b) \downarrow$	$avg(\Delta E_b) \downarrow$	$std(\Delta E_b) \downarrow$
γ -Al ₂ O ₃ (100)	Cu ₂₇	-0.56	0.27	-1.95	0.28	-9.67	0.48
	Cu ₃₈	-0.99	0.22	-2.59	0.54	-13.74	0.55
	Cu ₄₇	-1.21	0.32	-2.69	0.25	-16.83	0.40
	Cu ₅₅	-1.33	0.26	-0.80	0.19	1.48	0.35
γ -Al ₂ O ₃ (110)	Cu ₂₇	-0.42	0.30	-1.53	0.38	-8.00	0.42
	Cu ₃₈	-0.70	0.39	-1.85	0.45	-11.91	0.72
	Cu ₄₇	-0.96	0.55	-2.00	0.55	-14.74	0.93
	Cu ₅₅	-1.11	0.45	-0.15	0.16	3.34	0.55
α -Al ₂ O ₃ (0001)	Cu ₂₇	-0.27	0.20	-0.94	0.20	1.72	0.49
	Cu ₃₈	-0.10	0.23	-0.94	0.22	2.36	0.74
	Cu ₄₇	0.07	0.47	-1.05	0.23	2.17	0.31
	Cu ₅₅	-0.51	0.47	-1.61	0.19	2.25	1.08

Table 2: Ranking Metrics on Global Minimum Configurations

Surface	Size	RBO Kendall	q \uparrow $\tau\uparrow$	DP-UniAlCu	MACE-OMAT	MatterSim-v1.0.0-1M
γ -Al ₂ O ₃ (100)	Cu ₂₇	q		0.36	0.29	0.02
		τ		0.58	0.26	0.05
	Cu ₃₈	q		0.41	0.01	0.02
		τ		0.63	-0.42	0.07
	Cu ₄₇	q		0.70	0.21	0.79
		τ		0.51	0.70	0.46
	Cu ₅₅	q		0.44	0.30	0.26
		τ		0.48	0.48	0.39
	Cu ₂₇	q		0.37	0.13	0.06
		τ		0.60	0.51	0.46
γ -Al ₂ O ₃ (110)	Cu ₃₈	q		0.75	0.28	0.52
		τ		0.59	0.59	0.56
	Cu ₄₇	q		0.15	0.02	0.01
		τ		0.21	-0.27	-0.14
	Cu ₅₅	q		0.46	0.33	0.49
		τ		0.26	0.56	-0.01
	Cu ₂₇	q		0.14	0.28	0.01
		τ		0.50	0.61	-0.20
	Cu ₄₈	q		0.54	0.12	0.05
		τ		0.42	0.12	0.05
α -Al ₂ O ₃ (0001)	Cu ₄₇	q		0.43	0.51	0.46
		τ		0.27	0.81	0.61
	Cu ₅₅	q		0.43	0.25	0.01
		τ		-0.06	0.43	-0.21

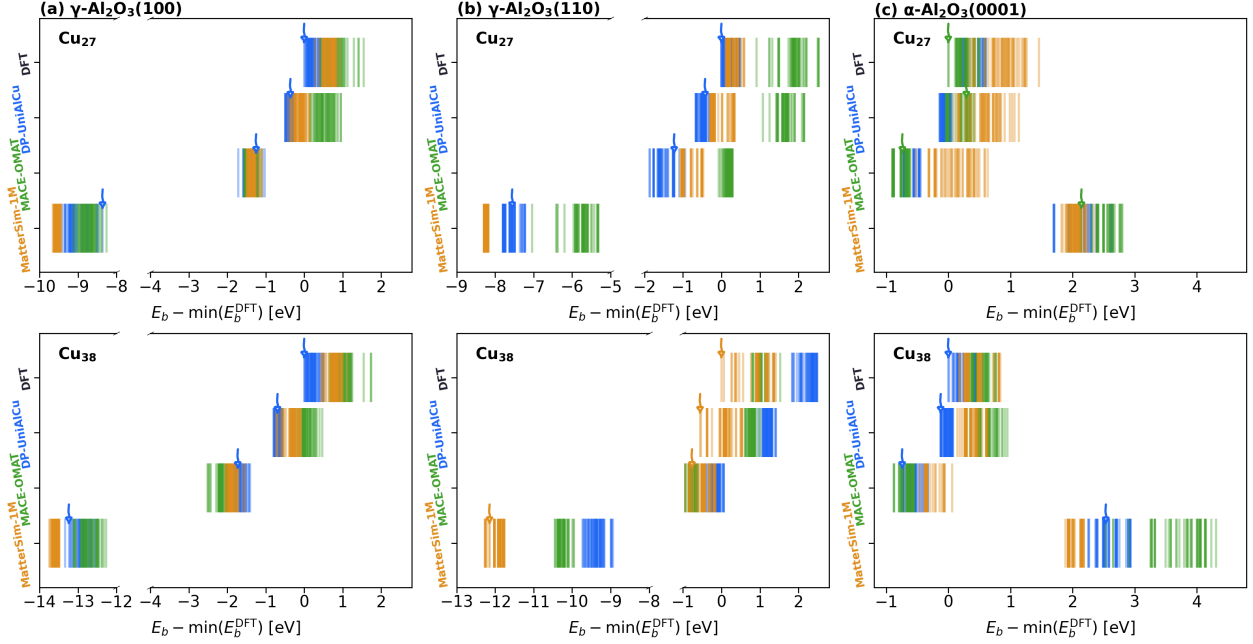


Figure 2: The low-energy configurations of Cu_{27} and Cu_{38} on $\gamma\text{-Al}_2\text{O}_3(100)$, $\gamma\text{-Al}_2\text{O}_3(110)$, and $\alpha\text{-Al}_2\text{O}_3(0001)$ by DFT, DP-UniAlCu (blue), MACE-OMAT (green), and MatterSim-v1.0.0-1M (orange). The DFT configurations are made up of structures obtained from MLIP-based global optimization. Each MLIP provides 50 structures for a given combination of the nanoparticle size and the supporting surface, forming a low-energy ensemble of 150 structures for each system. The arrows indicate the positions of the DFT-minimized global minimum configurations in spectra.

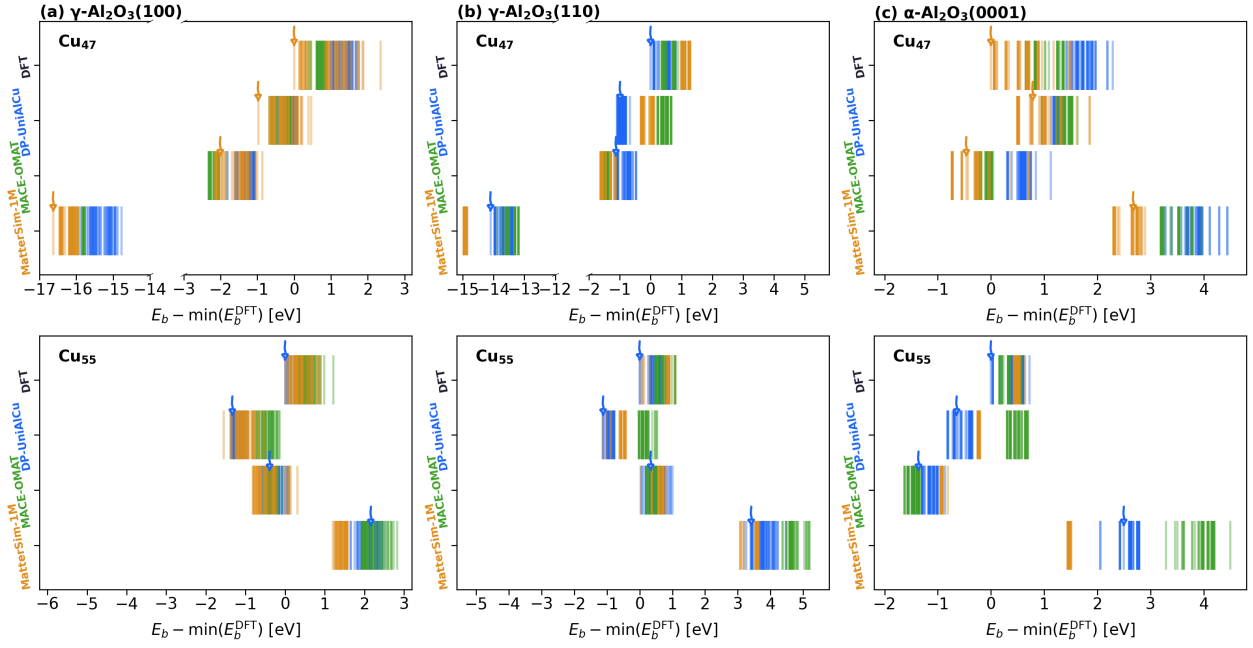


Figure 3: The low-energy configurations of Cu₄₇ and Cu₅₅ on γ -Al₂O₃(100), γ -Al₂O₃(110), and α -Al₂O₃(0001) by DFT, DP-UniAlCu (blue), MACE-OMAT (green), and MatterSim-v1.0.0-1M (orange). The DFT configurations are made up of structures obtained from MLIP-based global optimization. Each MLIP provides 50 structures for a given combination of the nanoparticle size and the supporting surface, forming a low-energy ensemble of 150 structures for each system. The arrows indicate the positions of the DFT-minimized global minimum configurations in spectra.

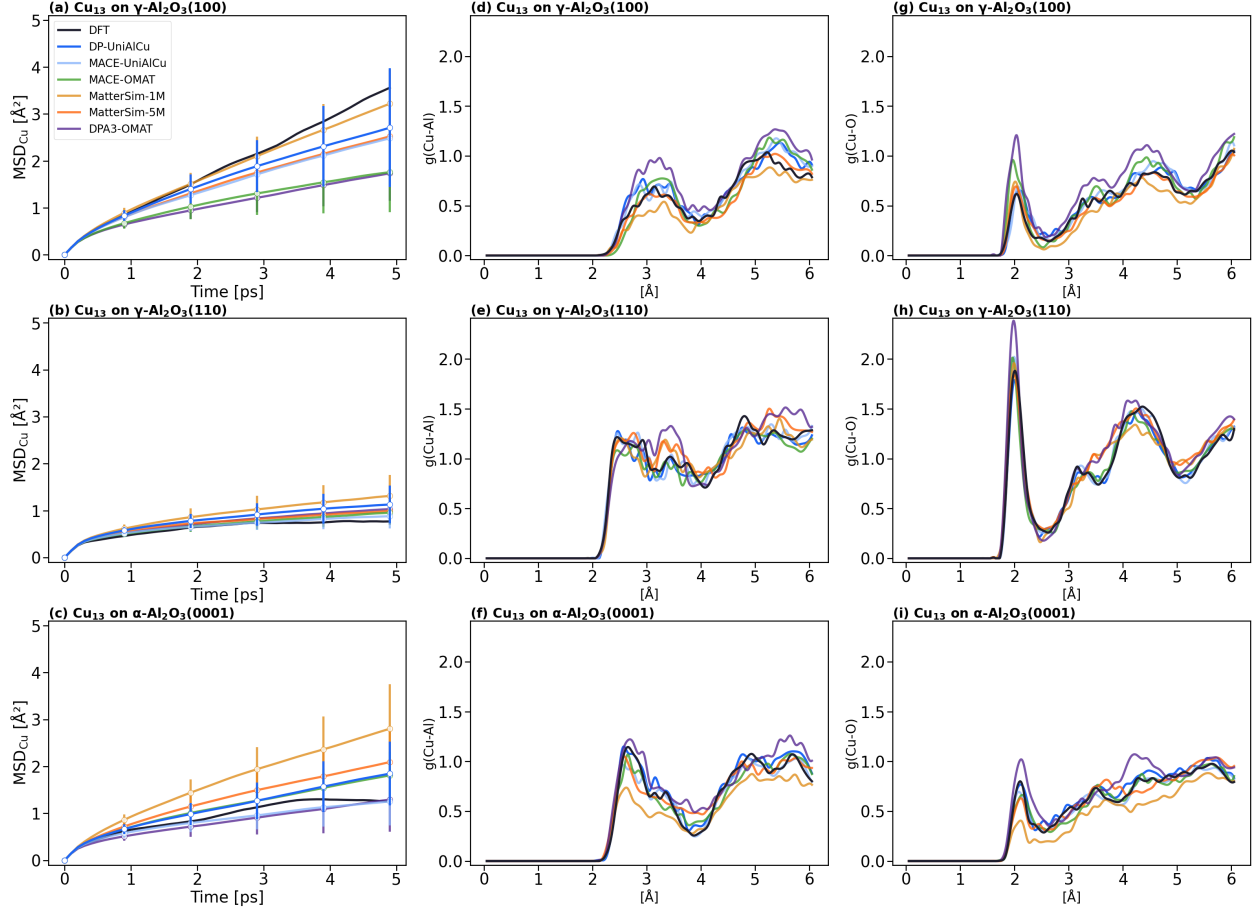


Figure 4: For each MLIP, 20 MD simulations starting from the same global minimum configuration of Cu_{13} but initialized from different velocities by Maxwell-Boltzmann distribution at 800 K are performed for 20 ps with a timestep of 2 fs. For AIMD, only one trajectory is performed with the same settings. (a)-(c) The mean square displacement of Cu atoms. The vertical bars are the standard deviations of 20 MD simulations by MLIPs. (d)-(f) The radial distribution functions of Cu-Al. (g)-(i) The radial distribution functions of Cu-O.

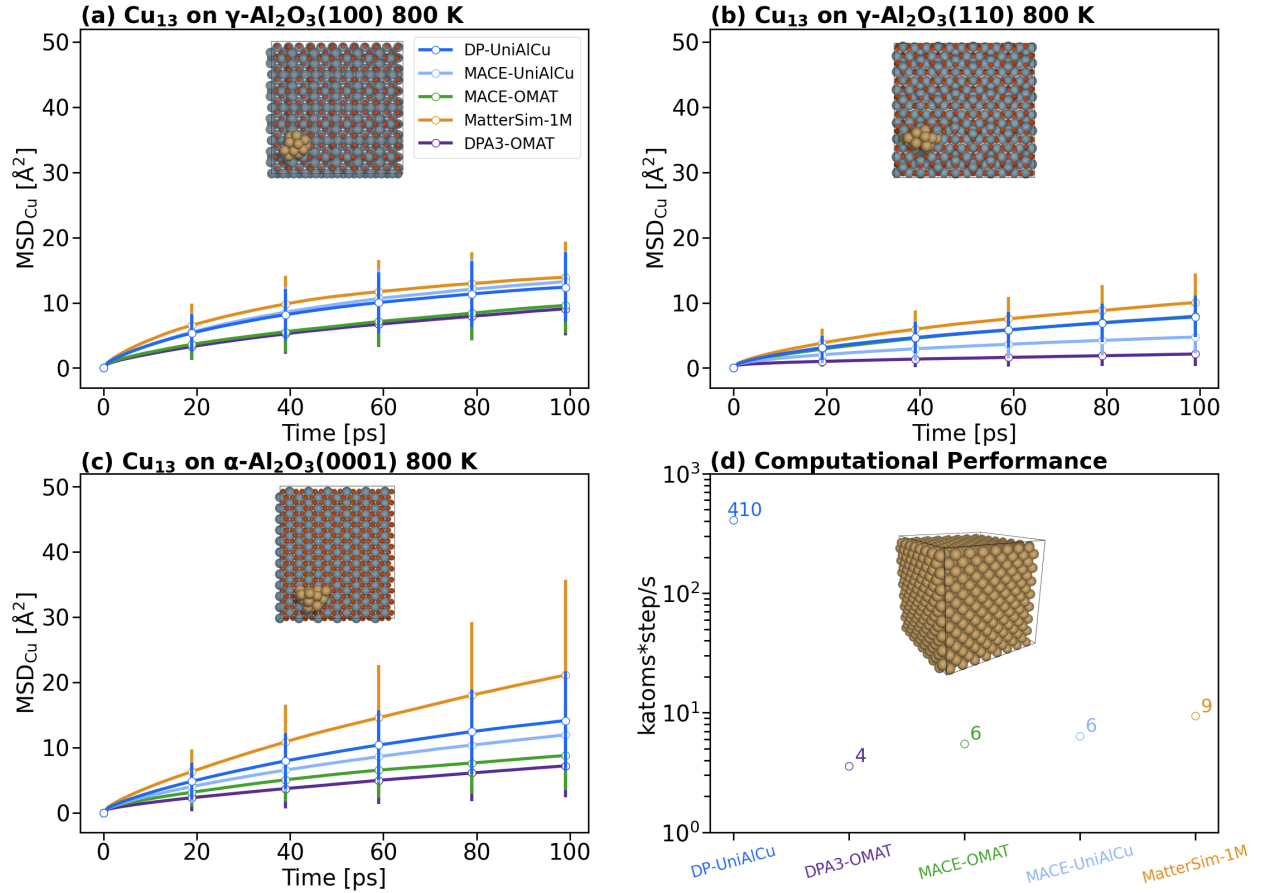


Figure 5: (a)-(c) The mean square displacement of Cu atoms for Cu₁₃ on three Al₂O₃ surfaces at 800 K. (d) The computational performance of DP-UniAlCu, DPA3-OMAT, MACE-OMAT, MACE-UniAlCu, and MatterSim-v1.0.0-1M models on the simulation of an FCC Cu bulk with 2048 atoms. The “katoms*step/s” is defined as the number of thousands of atoms processed per MD step per second. The inset panels show the initial structures of MD simulations.